International Journal of Nanoelectronics and Materials
IJNeaM
ISSN 1985-5761 | E-ISSN 2232-1535

Effect of Low Carbonization Temperature on Graphitic Properties of Palm Kernel Shell-Derived Carbon

Nurul Aishah Mohd Amran[a], Muhammad Mahyiddin Ramli[a,b,*], Norizah Abd Karim[c], Ismariza Ismail[d], Shazlina Johari[b], Anis Syafiqa Rosman[b], Nurul Huda Osman[e], Darminto[f], Ali H. Reshak[g,h]

[a]*Institute of Nano Electronic Engineering (INEE), Universiti Malaysia Perlis (UniMAP), 02600 Arau, Perlis, Malaysia*
[b]*Faculty of Electronic Engineering & Technology, Universiti Malaysia Perlis (UniMAP), 02600, Arau, Perlis, Malaysia*
[c]*Faculty of Mechanical Engineering & Technology, Universiti Malaysia Perlis (UniMAP), 02600, Arau, Perlis, Malaysia.*
[d]*Faculty of Chemical Engineering & Technology, Universiti Malaysia Perlis (UniMAP), 02600, Arau, Perlis, Malaysia*
[e]*Department of Physics, Faculty of Science, Universiti Putra Malaysia, 43400 Serdang, Selangor, Malaysia*
[f]*Department of Physics, Faculty of Science and Data Analytics, Institut Teknologi Sepuluh Nopember (ITS), Indonesia*
[g]*Physics Department, College of Science, University of Basrah, Basrah, post code 61004, Iraq*
[h]*Al-Kunooz University College, Basrah, Iraq*
**Corresponding author. E-mail: mmahyiddin@unimap.edu.my*

Received 4 Sept 2026, Revised 5 May 2026, Accepted 21 May 2026

ABSTRACT

This study explores the impact of carbonization temperature on the structural and defect properties of graphite prepared by means of palm kernel shell (PKS). Carbonization of the samples was carried out at 400, 500, and 600 °C with varying heating rates, and X-ray diffraction (XRD) and Raman spectroscopy were used. XRD analysis of the collected results showed the presence of broad (002) peaks in the range of 22–24°, suggesting the formation of incipient graphitic structures and decreased interlayer spacing with increasing temperature. The sharpest and highest-intensity (002) peak was found in the 600 °C sample carbonizing at 5 °C/min, indicating improved structural stability and ordering of carbon. With respect to the temperature increase, Raman microscopy revealed turbostratic ordering in graphite. Overall, these results demonstrate that low-temperature carbonization promotes incipient graphitic ordering in palm kernel shell (PKS). This approach provides a more sustainable and energy-efficient pathway for producing functional carbon materials, with potential applications in adsorption, catalysis, and energy storage.

Keywords: *Graphite, biomass*

1. INTRODUCTION

The growing demand for graphite has stimulated research into alternative production approaches beyond traditional natural sources. Graphite can be produced from a wide range of carbon-rich substrates, such as agricultural residues, fossil fuels, and wood, thereby making its synthesis more sustainable and increasing its future applicability [1]. Traditionally, coal and petroleum-based precursors have been the main sources for graphite production, however, these are non-renewable and environmentally taxing [2]. Graphite is a crystalline carbon type in the sense that well-ordered structures of carbon atoms are made up of a sort where carbon atoms are arranged in a hexagonal way and have consistent interlayer distances [3]. This high degree of structural order is typically achieved under extreme geological conditions of heat and pressure during metamorphism, or through artificial graphitization at elevated temperatures [4]. In contrast, turbostratic carbon represents a disordered variant of graphite. While it contains graphitic layers similar to those in crystalline graphite, the layers are misaligned, randomly stacked, or exhibit rotational disorder [5]. This leads to larger interlayer spacing and the absence of long-range three-dimensional order. Figure 1 shows the difference in the arrangement of the graphitic layers in graphite and turbostratic graphite carbon.

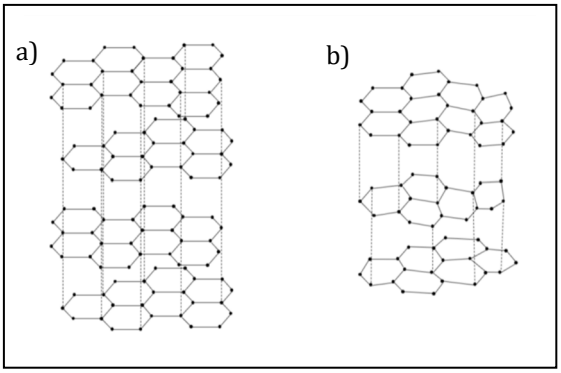

Figure 1. a) graphitic layer and b) turbostratic graphite layer.

In carbonization process, temperature plays a vital role in the production of graphite as it significantly affects the structural and chemical properties of the final product. The precursor undergoing incomplete or low-temperature carbonization or graphitization often retain turbostratic features, where carbon layers are present but lack perfect stacking [6]. Like graphite, it consists of layered carbon sheets, but these layers are misaligned or rotated, increasing the spacing between them. This misalignment creates numerous defects and edge sites, thereby increasing turbostratic graphite's surface area and porosity [7]. These features make it more reactive and useful for adsorption, catalysis, and energy storage [8]. It maintains some of graphite's stability and conductivity. The trade-off between order and disorder makes turbostratic graphite interesting in applications including activated carbon, batteries, and supercapacitors[9], [10]. In this study, we examined the carbonization using low temperatures at 400°C,500°C and 600°C. The carbonization temperatures of 400°C °C, 500 °C, and 600 °C were selected to investigate the progressive thermal transformation of lignocellulosic biomass into carbonaceous materials. The use of a lower temperature is intended to determine whether a turbostratic structure or crystalline graphite can form at low temperatures and to assess whether the process can lead to carbonization or graphitization.

2. THEORETICAL BACKGROUND

Malaysia is the second largest producer of oil palm, producing approximately 311 million tonnes of oil palm biomass annually[11]. Much of this biomass is left in plantations to decompose naturally or is burned openly, both of which can contribute to environmental issues such as air pollution. In addition, the accumulation of decomposing biomass might lure harmful insects, which could threaten the ecosystem and agricultural yield [12]. Thus, this significant amount of valuable biomass remains underutilized and wasted. At this stage, palm oil biomass residues, such as palm kernel shells (PKS), are suitable for conversion via mechanical and thermochemical processes, including pyrolysis, yielding high-value carbon materials such as graphite and related derivatives. [13]. In the background of the increasing interest toward graphite, a variety of research has been carried out on different raw materials for producing graphitic carbo,n such as sawdust, corn stalks, green tea waste, coconut coir and coconut stalk waste [14].

PKS is a carbon-rich biomass material primarily composed of cellulose (25 35%), hemicellulose (15–25%), and lignin (25–35%), with minor amounts of extractives and ash [15], [16], [17]. Among these, lignin plays the most significant role in carbon formation due to its aromatic and thermally stable structure, which enables it to yield more fixed carbon during pyrolysis [18]. Cellulose and hemicellulose decompose at relatively low temperatures. They produce gaseous products and relatively little char, but they are beneficial to the early formation of the carbon matrix [19]. The low ash content (generally 1–5%) in palm kernel shell (PKS) results in fewer inorganic residues, making PKS particularly well-suited for carbon-based applications. During pyrolysis in thermal treatment, hemicellulose decomposes first (approximately 200–260 °C), then cellulose (approximately 240–350 °C), and lastly lignin, which decomposes gradually from approximately 280 °C to 500 °C or higher. PKS has a relatively high lignin content and relatively low ash content, making it an excellent raw material for the production of graphite and other carbonaceous materials. Therefore, in this research, PKS was selected as a renewable precursor for graphite. The lignin content in PKS is believed to play a significant role in producing graphithe [20].

3. METHODOLOGY

The raw PKS was first dried at 60 °C for 30 minutes to remove surface moisture and then stored in airtight containers prior to thermal treatment. Carbonization was carried out under a nitrogen atmosphere using 200 g of PKS at temperatures of 400, 500, and 600 °C, with heating rates of 5, 10, and 15 °C/min and a fixed holding time of 3 hours. The holding time was kept constant, as it has little effect on atomic arrangement since structural ordering mainly occurs at the early stage of carbonization. However, holding time may still influence precursor interaction and structural development. Longer durations could improve graphitic ordering. Although this requires further study, a fixed holding time of 3 hours was used to maintain consistency and focus on the effects of temperature and heating rate.

After the carbonized materials were returned to room temperature and weighed, X-ray diffraction (XRD) was utilized to evaluate the structural properties of carbonized materials (i.e., crystallinity and carbon content) and the method of Raman spectroscopy was utilized to examine the structural order of the carbonized structure and the density of defects within the carbonized material.

4. DATA COLLECTION AND ANALYSIS

4.1. Sample Preparation

Palm kernel shell (PKS) used as the graphite precursor was obtained from FELCRA Berhad, Malaysia. Each piece weighed approximately 2–3 g. The PKS was dried in a rotary dryer at 60 °C for 30 minutes to remove surface moisture. After drying, the samples were stored in airtight containers to prevent moisture uptake before the carbonization process.

4.2. Carbonization Process

About 200g of PKS was weighed before undergoing carbonization process. A total of 9 samples were prepared to undergo difference carbonization temperature which was at 400 °C, 500°C and 600 °C with presence of nitrogen gas. Moderate temperatures (400–600 °C) were chosen to encourage aromatization and early graphitic ordering while limiting excessive mass loss and energy conserved. Additionally, a controlled heating rate and nitrogen atmosphere helped ensure gradual devolatilization and preserving the carbon structure. Each temperature parameter was then divided into 3 heating rates: 5 °C/min, 10 °C/min, and 15 °C/min. The process involves a 3-hour soak in a nitrogen atmosphere. Table 1 summarizes the parameters used in this process.

Table 1 Processing parameters for this process

Sample	Carbonization temperature (°C)	Heating rate (°C/min)
Raw	-	-
400/5	400	5
400/10	400	10
400/15	400	15
500/5	500	5
500/10	500	10
500/15	500	15
600/5	600	5
600/10	600	10
600/15	600	15

4.3. Characterization of Prepared Graphite

The yield of graphite was determined to evaluate the efficiency of the carbonization process. The resulting graphite was weighed once cooled to room temperature.
The structural characteristics of graphite were analyzed using X-ray diffraction (XRD). The powdered sample was mounted on a flat sample holder and scanned over a 2θ range of 5°–60° using Cu Kα radiation (λ = 1.5406 Å), operated at 40 kV and 30 mA. The scanning rate was set at approximately 2°/min. The diffraction patterns obtained were used to identify the crystalline phases and the degree of structural ordering.

Raman analysis was conducted to investigate the structural order and defect density of graphite. The sample was placed on a clean glass slide and analyzed using a Raman spectrometer with a 532 nm laser excitation source. The spectra were recorded over a range of 500–3000 cm^{-1}, with an acquisition time of 10 seconds per scan to capture the characteristic carbon bands.

5. DISCUSSION AND RESULTS

5.1. Yield of Carbonized Sample

Table 2 Yield of graphite at different carbonization temperatures and heating rates

Temperature (°C)	Heating Rate (°C/min)	Yield (%)
400	5	38
400	10	37
400	15	36
500	5	32

500	10	31
500	15	30
600	5	25
600	10	24
600	15	23

The yield of graphite decreased with increasing carbonization temperature. Carbonization at 400 °C resulted in the highest yields (36–38%), as the lower temperature limited the degradation of volatile constituents. These findings similar to [21] where lower carbonization temperatures (400 °C) result in higher char yields. However, such temperatures tend to preserve a predominantly amorphous carbon structure due to insufficient thermal energy for structural ordering.[22].

At 500 °C and 600 °C, the yield decreased significantly due to increased volatilization and decomposition of non-carbon elements (H, O, and light hydrocarbons), resulting in lower carbon residue [23]. At 600 °C conditions, the yield was lowest (23–25%) due to enhanced volatile loss and decrease in mass. But at this temperature, it promotes greater dehydrogenation and aromatic condensation, thereby forming a graphitic structure.

Among the heating rates tested, faster rates (10 and 15 °C/min) produced lower yields than the slower rate (5 °C/min). Among the heating rates examined, higher heating rates (10 and 15 °C/min) gave relatively lower yields compared to (5 °C/min). This is because of the high heating which causes abrupt devolatilization with high loss of mass and low recovery from carbon [24]. The slowest ramp (5 °C/min) consistently achieved higher yields which allowed gradual devolatilization condition and minimizing structural damages, while extended reaction time promotes aromatic condensation and facilitates π–π stacking between aromatic layers, leading to the formation of more ordered graphitic domains[25]. Hence, among the tested conditions, 600°C at 5 °C/min offers the best compromise for improved graphitic ordering.

5.2. XRD Analysis

Raw palm kernel shell (PKS) was analyzed as a reference to evaluating the effects of the carbonization process. The carbonized samples were characterized by XRD. The structural properties of the graphite were identified using the XRD curve. The interlayer spacing d(002) shows the extent of carbon interlayer disorder. The XRD diffractograms of the carbonized samples are treated at temperatures of 400 °C, 500 °C, and 600 °C under heating rates of 5 °C/min, 10 °C/min, and 15 °C/min, respectively.

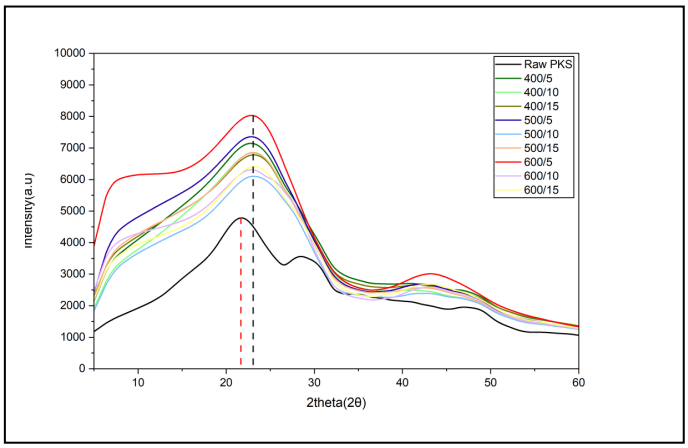

Figure 2. XRD patterns of raw PKS and carbonized PKS.

Broad, weak peaks are observed in the raw PKS powder (black line), indicating a predominantly amorphous structure. A noticeable hump at ~2θ≈30° is indicative of the accumulation of amorphous silica (SiO_2) or other inorganic mineral contaminants that are naturally found in lignocellulosic biomass[26]. After carbonization, that peak about 2θ ≈ 30° slowly recedes, indicative of the thermal decomposition of organic particles and the chemical transformation of inorganic minerals, which may undergo degradation, volatilization, or they are incorporated into the evolving carbon matrix [27].

By comparison, carbonized samples show a wide diffraction peak centered at 2θ ≈ 23–24° (black dashed line), which corresponds to (002) observation of turbostratic carbon, which is usually associated with disordered graphitic structures as the crystalline graphite observed at 26.7°[28]. As the carbonization temperature increases from 400 °C to 600 °C, the peak intensity increases more strongly. The 600/5 sample (red line) shows the highest peak intensity, indicating that the graphite is more ordered than in the other samples. The resultant increase in intensity represents not only the formation of more carbon layers in alignment with one another but also a more efficient way to stack graphite sheets [29]. More specifically, the peak

location seems to tilt a bit towards the higher angles with increasing temperature (from ~21° for raw PKS to ~23–24° for carbonized samples), this corresponds to lower interlayer spacing mentioned in Table 3. However, the crystalline graphite state at 26.7°, thus it is suggested that there is an incomplete process in graphitic structure [10]. Among all tested conditions, the 600/5 sample exhibits the highest degree of graphitic ordering, likely because the slower heating rate provides sufficient time for carbon atoms to rearrange into the turbostratic structure [30]. In summary, the carbonization temperature and heating rate have a significant effect on the crystallinity, graphitic ordering, and overall structure of PKS-derived carbon [31]. The value of interlayer spacing d(002) for each sample is indicated in Table 3.

Table 3 Interlayer Spacing d(002) of Carbonized PKS

Sample	2theta (2θ)	d(002) (nm)
400/5	23.0	0.387
400/10	23.0	0.387
400/15	22.5	0.396
500/5	23.5	0.377
500/10	23.0	0.387
500/15	22.5	0.396
600/5	24.0	0.370
600/10	23.5	0.379
600/15	23.0	0.387

According to the interlayer spacing determined in Table 3, d(002) values were still relatively high (0.387–0.396 nm) at 400 °C, in association with the highly disordered carbon structure and low graphitic stacking. The temperature raised to 500 °C causes lower interlayer spacing, where the 500/5 sample gives 0.3768 nm, indicating the onset of ordered carbon layer formation. At sample 600/5 the significant improvement appears mainly with respect to the slowest heating, as the d(002) value decreases to 0.370 nm. This reduction in interlayer gap, and the increase of peak to 2θ = 24° demonstrates that the approach toward ideal graphite-stacked structure is closer (0.335 nm) and the stacking of graphite layers becomes better [32], [33]. More rapid heating rates at 600/10 and 600/15, on the other hand, lead to larger d(002) values (0.379 nm and 0.387 nm), meaning the structural ordering is not as good. Out of the various conditions tested, carbonization at 600 °C with a heating rate of 5 °C/min led to increased turbostratic carbon structure formation as evidenced by a higher intensity of peaks, displayed by X-ray diffraction (XRD) patterns.

5.3. Raman Analysis

Raman spectroscopy was employed to investigate the phase characteristics of carbon-based materials. As a phase analysis technique, Raman offers important information on the degree of crystalline, defect density, and the structural ordering of graphitic domains. Figure 3 (a), (b) and (c) present the Raman spectra of carbonized samples produced at 400 °C, 500 °C, and 600 °C under different heating rates of 5°C/min, 10°C/min, and 15 °C/min, respectively.

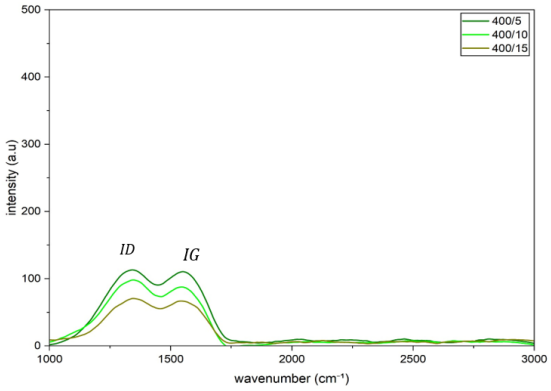

Figure 3. a) Raman spectra for carbonized PKS at 400°C.

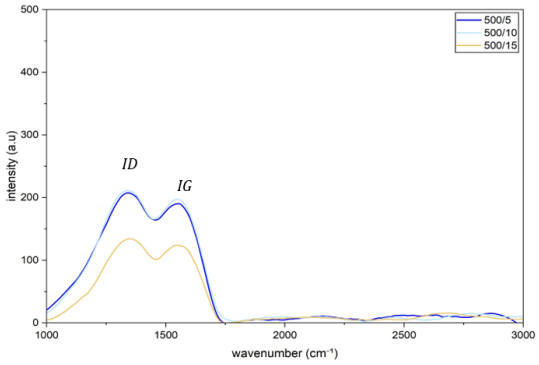

Figure 3. b) Raman spectra for carbonized PKS for 500°C.

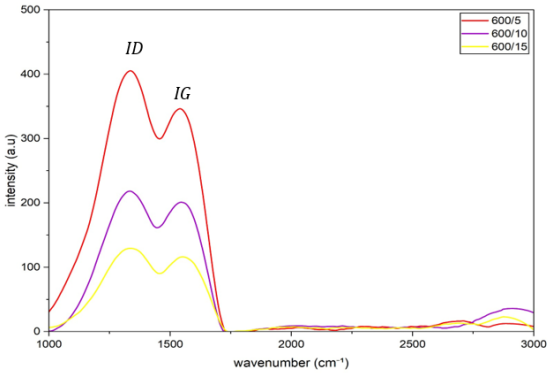

Figure 3. c) Raman spectra for carbonized PKS at 600°C.

From Figure 3 (a), (b) and (c) the Raman spectra exhibit the characteristic D band (~1350 cm^{-1}) and G band (~1580 cm^{-1}), corresponding to structural defect and graphitic structure, respectively. The presence of the G band confirms the development of graphitic carbon structures, which arise from the in-plane vibration of sp^2-bonded carbon atoms in a two-dimensional hexagonal lattice [34]. The D band originates from the breathing modes of sp^2 carbon rings, commonly regarded as defects or lattice disorder within the carbon framework [35].

From Figure 3(a), the sample carbonized at 400 °C exhibits the weakest peak intensity, whereas Figure 3(b) at 500 °C shows a moderate intensity, and Figure 3(c) at 600 °C displays the most pronounced peak corresponding to the highest degree of carbonization. Regarding the heating rates, the sample treated at 5 °C/min exhibits the highest peak intensity compared with those at 10 and 15 °C/min. This outcome suggests that slower heating allows sufficient time for carbon atoms to rearrange into more ordered configurations, thereby enhancing structural development. These findings agree with the previously discussed XRD analysis, confirming that the most well-developed graphitic ordering is obtained at 600 °C with a heating rate of 5 °C/min.

However, in general, a higher G band intensity and a lower D band are interpreted as indicating that the carbon has a more graphitic structure [36]. The spectra presented in Fig 4(a), (b) and (c) reveal a somewhat contradictory trend. This phenomenon can be attributed to the aggregation behaviour of amorphous carbon structures that initially possess limited graphitic structure [37]. Another possible reason is that the graphite may possess a well-ordered structure, but the crystallites are small, with numerous edge boundaries and a high density of lattice defects [38], [39]. Thus, it can be hypothesized that the graphitic structure obtained contributes to the formation of turbostratic carbon.

Table 4 The ID/IG value for carbonized PKS

Sample	**400/5**	**400/10**	**400/15**	**500/5**	**500/10**	**500/15**	**600/5**	**600/10**	**600/15**
ID/IG	0.85	0.88	0.96	0.88	0.92	0.97	0.88	0.86	0.98

The Raman spectra of the carbonized samples exhibit ID/IG values ranging from 0.85 to 0.98, indicating the formation of predominantly turbostratic carbon structures with partial graphitic ordering. In general, the presence of the D band reflects structural defects and disorder, while the G band corresponds to sp^2-bonded carbon domains. The relatively high ID/IG ratios observed across all samples suggest that, although some degree of sp^2 carbon network formation has occurred, the carbon structure remains largely disordered and has not reached a fully graphitized state [40].

A mild dependence on processing conditions is observed, with lower heating rates yielding lower ID/IG values, indicating better structural ordering due to slower devolatilization and improved aromatic condensation. Conversely, higher heating rates (e.g., 15 °C/min) lead to elevated ID/IG values, suggesting increased defect density, likely caused by rapid release of volatiles and limited time for carbon network rearrangement. The effect of temperature within the studied range (400–600 °C) is less significant, indicating that this range mainly supports initial carbonization and the formation of early-stage graphitic domains rather than complete graphitization.

CONCLUSIONS

The present study shows that carbonization of palm kernel shell up to 600 °C at a heating rate of 5 °C/min promotes incipient graphitic ordering, and a fully crystalline graphite structure is not achieved. The yield decreased from 38% at 400 °C to 23% at 600 °C due to extensive devolatilization, which in turn facilitates aromatization and enhances carbon structural ordering. XRD and Raman analyses confirm the formation of layered graphitic-like structures with increased interlayer spacing and lattice defects compared to crystalline graphite, indicating the presence of turbostratic carbon.

ACKNOWLEDGEMENT

The authors would like to thank the Ministry of Higher Education and UniMAP for financial support through the RESERVE Grant (9001-00796).

REFERENCES

[1] R. Yadav, A. K. Sharma, and S. Sharma, "Advance Development in Natural Graphite Material and Its Applications: A Review," Feb. 01, 2024, *Springer Science and Business Media Deutschland GmbH*. doi: 10.1007/s42461-024-01167-z.

[2] N. Ahmad, "An Overview of Activated Carbon Preparation from Various Precursors," *Scientific Research Journal*, vol. 20, no. 1, pp. 51–89, Mar. 2023, doi: 10.24191/srj.v20i1.20963.

[3] Y. Ge *et al.*, "Graphite-hexagonal diamond hybrid with diverse properties," *Appl. Phys. Rev.*, vol. 10, no. 2, Jun. 2023, doi: 10.1063/5.0151183.

[4] D. Song, J. Li, Z. Wang, and C. Zhao, "Performance of graphite felt as anodes in the electro-Fenton oxidation systems: Changes in catalysis, conductivity and adsorption properties," *Appl. Surf. Sci.*, vol. 532, Dec. 2020, doi: 10.1016/j.apsusc.2020.147450.

[5] P. Kokmat, P. Surinlert, and A. Ruammaitree, "Growth of High-Purity and High-Quality Turbostratic Graphene with Different Interlayer Spacings," *ACS Omega*, vol. 8, no. 4, pp. 4010–4018, Jan. 2023, doi: 10.1021/acsomega.2c06834.

[6] N. Richter *et al.*, "Robust Two-Dimensional Electronic Properties in Three-Dimensional Microstructures of Rotationally Stacked Turbostratic Graphene," *Phys. Rev. Appl.*, vol. 7, no. 2, Feb. 2017, doi: 10.1103/PhysRevApplied.7.024022.

[7] I. L. Spain, "Electronic Transport Properties of Graphite, Carbons, and Related Materials," in *Chemistry and Physics of Carbon*, vol. 16, 2021, p. 186. doi: 10.1201/9781003209065-2.

[8] D. B. Schuepfer *et al.*, "Assessing the structural properties of graphitic and non-graphitic carbons by Raman spectroscopy," *Carbon N. Y.*, vol. 161, pp. 359–372, May 2020, doi: 10.1016/j.carbon.2019.12.094.

[9] P. Murugan, R. D. Nagarajan, B. H. Shetty, M. Govindasamy, and A. K. Sundramoorthy, "Recent trends in the applications of thermally expanded graphite for energy storage and sensors - a review," Nov. 21, 2021, *Royal Society of Chemistry*. doi: 10.1039/d1na00109d.

[10] T. Jalalabadi, J. Wu, B. Moghtaderi, N. Sharma, and J. Allen, "A new approach to turbostratic carbon production via thermal salt-assisted treatment of graphite," *Fuel*, vol. 348, Sep. 2023, doi: 10.1016/j.fuel.2023.128489.

[11] L. M. Terry *et al.*, "Bio-oil production from pyrolysis of oil palm biomass and the upgrading technologies: A review," Jan. 01, 2021, *KeAi Publishing Communications Ltd.* doi: 10.1016/j.crcon.2021.10.002.

[12] N. Khalid, N. A. Abdul Rahman, C. Wai Yan, and Z. Idris, "The Palm Oil Export Market," 2025. doi: DOI:10.4324/9781003518600.

[13] S. Kaniapan, S. Hassan, H. Ya, K. P. Nesan, and M. Azeem, "The utilisation of palm oil and oil palm residues and the related challenges as a sustainable alternative in biofuel, bioenergy, and transportation sector: A review," Mar. 02, 2021, *MDPI AG*. doi: 10.3390/su13063110.

[14] S. Sankar *et al.*, "Biomass-derived ultrathin mesoporous graphitic carbon nanoflakes as stable electrode material for high-performance supercapacitors," *Mater. Des.*, vol. 169, May 2019, doi: 10.1016/j.matdes.2019.107688.

[15] J. R. García, U. Sedran, M. A. A. Zaini, and Z. A. Zakaria, "Preparation, characterization, and dye removal study of activated carbon prepared from palm kernel shell," *Environmental Science and Pollution Research*, vol. 25, no. 6, pp. 5076–5085, Feb. 2018, doi: 10.1007/s11356-017-8975-8.

[16] E. Baffour-Awuah, S. A. Akinlabi, T. C. Jen, S. Hassan, I. P. Okokpujie, and F. Ishola, "Characteristics of Palm Kernel Shell and Palm Kernel Shell-Polymer Composites: A Review," *IOP Conf. Ser. Mater. Sci. Eng.*, vol. 1107, no. 1, p. 012090, Apr. 2021, doi: 10.1088/1757-899x/1107/1/012090.

[17] O. M. Ikumapayi and E. T. Akinlabi, "Composition, characteristics and socioeconomic benefits of palm kernel shell exploitation-an overview," 2018, *Asian Network for Scientific Information*. doi: 10.3923/jest.2018.220.232.

[18] M. Muddasar, M. Culebras, and M. N. Collins, "Lignin and its carbon derivatives: Synthesis techniques and their energy storage applications," Dec. 01, 2024, *Elsevier Ltd*. doi: 10.1016/j.mtsust.2024.100990.

[19] X. Chen, Z. Qu, Z. Liu, and G. Ren, "Mechanism of Oxidization of Graphite to Graphene Oxide by the Hummers Method," *ACS Omega*, vol. 7, no. 27, pp. 23503–23510, 2022, doi: 10.1021/acsomega.2c01963.

[20] N. H. Jabarullah, A. S. Kamal, and R. Othman, "A modification of palm waste lignocellulosic materials into biographite using iron and nickel catalyst," *Processes*, vol. 9, no. 6, Jun. 2021, doi: 10.3390/pr9061079.

[21] J. Oladejo, K. Shi, X. Luo, G. Yang, and T. Wu, "A review of sludge-to-energy recovery methods," Jan. 01, 2019, *MDPI AG*. doi: 10.3390/en12010060.

[22] L. Xie, L. Gou, D. Xu, K. Kapusta, L. Dai, and Y. Wang, "Coupling influences of organic components and temperature on nitrogen transformation and hydrochar characterization during hydrothermal carbonization of sewage sludge," *Science of the Total Environment*, vol. 866, Mar. 2023, doi: 10.1016/j.scitotenv.2022.161354.

[23] Y. Wang, T. Wang, Q. Gu, and J. Shang, "Adsorption Removal of NO2 Under Low-Temperature and Low-Concentration Conditions: A Review of Adsorbents and Adsorption Mechanisms," Feb. 05, 2025, *John Wiley and Sons Inc*. doi: 10.1002/adma.202401623.

[24] A. Phounglamcheik *et al.*, "Effects of Pyrolysis Conditions and Feedstocks on the Properties and Gasification Reactivity of Charcoal from Woodchips," *Energy and Fuels*, vol. 34, no. 7, pp. 8353–8365, Jul. 2020, doi: 10.1021/acs.energyfuels.0c00592.

[25] Y. Nakamura, T. Yoshino, and M. Satish-Kumar, "An experimental kinetic study on the structural evolution of natural carbonaceous material to graphite," *American Mineralogist*, vol. 102, no. 1, pp. 135–148, Jan. 2017, doi: 10.2138/am-2017-5733.

[26] A. Mourhly, M. Khachani, A. El Hamidi, M. Kacimi, M. Halim, and S. Arsalane, "The synthesis and characterization of low-cost mesoporous silica SiO2 from local pumice rock," *Nanomaterials and Nanotechnology*, vol. 5, 2015, doi: 10.5772/62033.

[27] M. Labus, I. Matyasik, and K. Ziemianin, "Thermal Decomposition Processes in Relation to the Type of Organic Matter, Mineral and Maceral Composition of Menilite Shales," *Energies (Basel).*, vol. 16, no. 11, Jun. 2023, doi: 10.3390/en16114500.

[28] X. Zhang *et al.*, "Observation of carbon nanostructure and evolution of chemical structure from coal to graphite by high temperature treatment, using componential determination, X-ray diffraction and high-resolution transmission electron microscope," *Fuel*, vol. 332, Jan. 2023, doi: 10.1016/j.fuel.2022.126145.

[29] A. Vlahov, "XRD graphitization degrees: A review of the published data and new calculations, correlations, and applications," *Geologica Balcanica*, vol. 50, no. 1, pp. 11–35, Apr. 2021, doi: 10.52321/GeolBalc.50.1.11.

[30] L. Lai, J. Li, Y. Deng, Z. Yu, L. Wei, and Y. Chen, "Carbon and Carbon/Metal Hybrid Structures Enabled by Ultrafast Heating Methods," Nov. 01, 2022, *John Wiley and Sons Inc*. doi: 10.1002/sstr.202200112.

[31] C. Zhao *et al.*, "Effects of the carbonization temperature and intermediate cooling mode on the properties of coal-based activated carbon," *Energy*, vol. 273, Jun. 2023, doi: 10.1016/j.energy.2023.127177.

[32] R. Ganjoo, S. Sharma, A. Kumar, and M. M. A. Daouda, "Activated Carbon: Fundamentals, Classification, and Properties," in *Activated Carbon*, The Royal Society of Chemistry, 2023, pp. 1–22. doi: 10.1039/bk9781839169861-00001.

[33] M. Abdillah, A. Farid, A. Lim, T. Zheng, T. Tsubota, and Y. Andou, "Catalytic graphitization of biomass-derived ethanosolv lignin multiple layers of graphitic carbon. These findings might pave the way for future high-value," 2023.

[34] J. George, S. Upadhyay, and M. Balachandran, "Exploration of Graphene Layers in Various Carbon Materials by Raman Spectroscopic Techniques," *Mapana Journal of Sciences*, vol. 20, no. 4, pp. 65–81, Oct. 2021, doi: 10.12723/mjs.59.5.

[35] N. Umada, K. Kanda, M. Niibe, Y. Hirata, N. Ohtake, and H. Akasaka, "Oriented sp2 bonded carbon structure of hydrogenated amorphous carbon films," *Diam. Relat. Mater.*, vol. 131, Jan. 2023, doi: 10.1016/j.diamond.2022.109533.

[36] W. Liu and G. Speranza, "Tuning the Oxygen Content of Reduced Graphene Oxide and Effects on Its Properties," *ACS Omega*, vol. 6, no. 9, pp. 6195–6205, Mar. 2021, doi: 10.1021/acsomega.0c05578.

[37] P. Zhang, J. Fan, Y. Wang, Y. Dang, S. Heumann, and Y. Ding, "Insights into the Role of Defects on the Raman Spectroscopy of Carbon," Dec. 2023. [Online]. Available: https://ssrn.com/abstract=4652843

[38] J. Li, Y. Qin, Y. Chen, Y. Song, and Z. Wang, "HRTEM observation of morphological and structural evolution of aromatic fringes during the transition from coal to graphite," *Carbon N. Y.*, vol. 187, pp. 133–144, Feb. 2022, doi: 10.1016/j.carbon.2021.11.006.

[39] L. Yuan, Q. Liu, J. P. Mathews, H. Zhang, and Y. Wu, "Quantifying the Structural Transitions of Chinese Coal to Coal-Derived Natural Graphite by XRD, Raman Spectroscopy, and HRTEM Image Analyses," *Energy and Fuels*, vol. 35, no. 3, pp. 2335–2346, Feb. 2021, doi: 10.1021/acs.energyfuels.0c04019.